Parametric Reduced Order Model Approach for Rapid Dynamic Loads Prediction

Michele Castellani[a,b,*], Yves Lemmens[a], Jonathan E. Cooper[b]

[a]*Aerospace Centre of Competence, Siemens PLM Software (Belgium), Interleuvenlaan 68, 3001 Leuven, Belgium*
[b]*Department of Aerospace Engineering, Faculty of Engineering, University of Bristol, Queen's Building, University Walk, BS8 1TR Bristol, United Kingdom*
[*]Corresponding author
E-mail address: michele.castellani@bristol.ac.uk

ABSTRACT

A parametric reduced order methodology for loads estimation is described that produces a fast and accurate prediction of gust and manoeuvre loads for different flight conditions and structural parameter variations. The approach enables efficient prediction of the peak loads whilst maintaining the correlated time histories for different loads. It is then possible to determine correlated loads plots with reduced computation without losing accuracy. The effectiveness of the methodology is demonstrated by considering loads arising from families of gusts and pitching manoeuvres acting upon a numerical transport aircraft aeroservoelastic model with varying flight conditions and structural properties.

Keywords: gust loads; state-space aeroelasticity; Reduced Order Model; flexible aircraft; correlated loads

Nomenclature

$\boldsymbol{A}$, $\boldsymbol{B}$, $\boldsymbol{C}$, $\boldsymbol{D}$	State-space system matrices of Full Order Model
$\boldsymbol{A_r}$, $\boldsymbol{B_r}$, $\boldsymbol{C_r}$, $\boldsymbol{D_r}$	State-space system matrices of Reduced Order Model
$\boldsymbol{A_a}$	Matrix coefficients of Rational Function Approximation of aerodynamics
$\boldsymbol{A_g}$	Matrix coefficients of Rational Function Approximation of gust aerodynamics
$\boldsymbol{B_a}$	Matrix coefficients of Rational Function Approximation of aerodynamics
$\boldsymbol{B_g}$	Matrix coefficients of Rational Function Approximation of gust aerodynamics
$\boldsymbol{C_a}$	Matrix coefficients of Rational Function Approximation of aerodynamics
$\boldsymbol{C_g}$	Matrix coefficients of Rational Function Approximation of gust aerodynamics
$\boldsymbol{C_{hh}}$	Generalized damping matrix
$\boldsymbol{D_0}, \boldsymbol{D_1}, \boldsymbol{D_2}$	Matrix coefficients of Rational Function Approximation of aerodynamics
$\boldsymbol{D_{0g}}, \boldsymbol{D_{1g}}, \boldsymbol{D_{2g}}$	Matrix coefficients of Rational Function Approximation of gust aerodynamics
$\boldsymbol{D_{0c}}, \boldsymbol{D_{1c}}, \boldsymbol{D_{2c}}$	Matrix coefficients of Rational Function Approximation of control surface aerodynamics
$\mathcal{F}$	Functional of the extended Rational Function Approximation
G_h	Open-loop actuator transfer function
h	Altitude
H_C	Closed-loop actuator transfer function
i	Imaginary unit
$\boldsymbol{I}$	Identity matrix
k	Reduced frequency
k_c	Gain of closed-loop actuator transfer function
k_h	Hydraulic gain
$\boldsymbol{K}$	Stiffness matrix in physical coordinates
$\boldsymbol{K_{hh}}$	Generalized stiffness matrix
l_a	Aerodynamic reference length
M	Mach number
$\boldsymbol{M}$	Mass matrix in physical coordinates
$\boldsymbol{M_{hh}}$	Generalized mass matrix
n_a	Number of aerodynamic poles

n_d	Number of parameters of the model
n_h	Number of generalized coordinates
n_k	Number of reduced frequencies
n_p	Number of sampling points
n_r	Order of Reduced Order Model
n_z	Vertical load factor
N	Order of Full Order Model
p	Complex reduced frequency
$\boldsymbol{p}$	Vector of parameters of the model
q_∞	Dynamic pressure
$\boldsymbol{q_h}$	Generalized coordinates
$\boldsymbol{Q_{AA}}$	Aerodynamic forces matrix on structural degrees of freedom due to structural displacements
$\boldsymbol{Q_{Ag}}$	Aerodynamic forces matrix on structural degrees of freedom due to gust
$\boldsymbol{Q_{hh}}$	Generalized aerodynamic forces matrix due to structural displacements
$\boldsymbol{Q_{hg}}$	Generalized aerodynamic forces matrix due to gust
$\boldsymbol{Q_{hc}}$	Generalized aerodynamic forces matrix due to control surfaces
s	Laplace variable
$\boldsymbol{T}$	Generalized basis matrix for structural modifications
$\boldsymbol{T_B}$	Balanced truncation basis matrix
V	Airspeed
$\boldsymbol{V}$	Left reduced order basis matrix
$\boldsymbol{W}$	Right reduced order basis matrix
V_A/M_A	Design manoeuvering speed/Mach number
V_C/M_C	Design cruise speed/Mach number
V_D/M_D	Design diving speed/Mach number
$\boldsymbol{u}$	State-space model input vector
u_c	Pilot command input
w_{ij}	Weighting factor of the optimization process for the extended Rational Function Approximation
w_g	Gust velocity
$\boldsymbol{x}$	State-space states vector of Full Order Model
$\boldsymbol{x_r}$	State-space states vector of Reduced Order Model
$\boldsymbol{x_g}$	Gust aerodynamics states vector
$\boldsymbol{x_a}$	Aerodynamic states vector
$\boldsymbol{x_g}$	Gust aerodynamics states vector
$\boldsymbol{y}$	State-space model output vector
β_l	Aerodynamic poles of Rational Function Approximation
δ	Control surface deflection
ε_{ij}	Normalized squared error between tabulated and approximated *i-j* terms of generalized aerodynamic matrix
$\mathbf{\Delta M}$	Additional mass matrix containing structural modifications
$\mathbf{\Delta K}$	Additional stiffness matrix containing structural modifications
$\mathbf{\Phi}$	Matrix of eigenvectors
$\mathbf{\Phi_{RB}}$	Matrix of rigid body modes
ζ_h	Hydraulic damping
ω_h	Hydraulic natural frequency

Abbreviations

DLM	Doublet Lattice Method
DOF	Degree Of Freedom
FOM	Full Order Model
GAF	Generalized Aerodynamic Forces
IQ	Interesting Quantity
LC	Load Case
LTI	Linear Time Invariant

MAC Modal Assurance Criterion
MTOW Maximum Take-Off Weight
PROM Parametric Reduced Order Model
RFA Rational Function Approximation
RMSE Root mean square error
ROB Reduced Order Basis
ROM Reduced Order Model
SVD Singular Value Decomposition

1. Introduction

Loads calculations play an important part across much of the design and development of an aircraft, and have an impact upon structural design, aerodynamic characteristics, weight, flight control system design and performance. They determine the most extreme stress levels, fatigue damage and damage tolerance. The certification of large commercial aircraft is covered by the EASA CS-25 documents [1] which define a range of load cases that has to be accounted for, and are a primary prerequisite for assuring structural integrity over the operating environment of the aircraft. Loads requirements are defined in the context of the flight envelope. The regulations require that enough points on, or within, the boundary of the flight envelope are investigated to ensure that the most extreme loads for each part of the aircraft structure are identified.

The flight conditions which provide the largest aircraft loads are not known a-priori. Therefore the aerodynamic and inertial forces have to be calculated at a large number of conditions to give an estimate of the maximum loads, and hence stresses, that the aircraft will experience in service. It is of great interest for aircraft design to identify which are the critical loading events and at what design configuration and flight conditions they occur. A typical aircraft loads design process involves monitoring many of so-called Interesting Quantities (IQs) (e.g. bending moments, torques, accelerations etc.) for a wide range of different load cases that the aircraft is likely to experience in-flight and on the ground. Each "loads loop" simulates the response of a numerical aeroelastic aircraft model to these loads and determine the critical cases, and these results are fed into the structural design. Such a process is extremely time consuming and furthermore, has to be repeated every time that there is an update in the aircraft structure.

It is usual to determine the extreme loads cases for 1D (single IQs) and 2D (correlated IQs) events. In the latter case, pairs of IQ response time histories (e.g. bending moment and torque at a single position on the aircraft) are visualized against each other for a range of different load cases. The extreme vertices of the envelope encompassing these correlated time histories characterizes the critical load cases that are then used to perform stress calculations.

There is interest in developing methodologies that are able to determine the worst case gust loads without excessive computation; however, approaches such as Matched Filter Theory [2], Statistical Discrete Gust [3] and Evolutionary Algorithm [4] methods all determine arbitrary gust time histories that give the worst 1D response. The time domain approaches defined in the airworthiness regulations [1],[5] are based upon finding the tuned "1 - Cosine" gust that causes the worst response. Previous work in the FFAST EU FP7 project [6],[7],[8] investigated the use of several surrogate models and optimization methods for fast and efficient prediction of the worst case gust loads for each IQ of a large transport aircraft model. It was shown that considerable savings in computational time can be made without sacrificing accuracy; however, the IQs were dealt with independently. Recent work [9],[10] have investigated approaches to determine reduced order models of correlated loads based upon the use of the Singular Value Decomposition (SVD), whereas a robust performance approach was considered in [11]. Little work has considered correlated gust responses.

In this work, an approach for rapid loads estimation based on Parametric Model Order Reduction (PMOR) will be described that determines a Reduced Order Model (ROM) able to predict IQs time histories for different flight conditions and design parameter variations. The effectiveness of the developed method is demonstrated by considering loads due to gusts and pitching manoeuvres for a simulated aeroservoelastic model of a generic transport aircraft. It is shown for the test cases considered that a good accuracy is maintained with a significant reduction in computational time. The analyses focus on symmetric load cases, but the method does not have any limitation preventing its applicability to lateral gusts and anti-symmetric manoeuvres as well.

2. Aeroservoelastic model

The procedure described in this paper has been applied to the discrete gust response and pitching manoeuvre simulation of a generic aircraft, representative of a modern airliner, whose main features are summarized in Table 1.

Table 1. Main features of the aircraft model.

Property	Value
Length	67*m*
Wingspan	65*m*
Height	17*m*
Wing area	445m^2
Mean Aerodynamic Chord	6.07*m*
MTOW	268*tons*
Max operating altitude	43000*ft*
V_A-M_A	142*m/s*-0.82
V_C-M_C	172*m/s*-0.89
V_D-M_D	188*m/s*-0.95
$n_{z,max}$	2.5*g*
$n_{z,min}$	-1*g*

The aircraft model was developed as part of the FFAST FP7 project. The structural model is a FE stick model where the fuselage, wing, tailplanes and engine pylons are represented by beam elements in the FE solver Nastran. The model includes both distributed and lumped masses for the systems, furniture, payload, fuel and engines. The aerodynamic model is a Doublet Lattice Method (DLM) [12] mesh where each lifting surface is modelled as a flat plate. The interface between structure and aerodynamics is based upon the Infinite Plate Spline method [13]. The aerostructural mesh is shown in Fig. 1. The control surfaces (elevator, ailerons and rudder) are modelled only in the aerodynamic mesh in order to introduce their aerodynamic forces contribution as inputs to the aeroservoelastic model. The control surfaces are assumed controlled through servo-hydraulic actuators, whose transfer functions are known following a linearization of the originally non-linear equations around the neutral operating point.

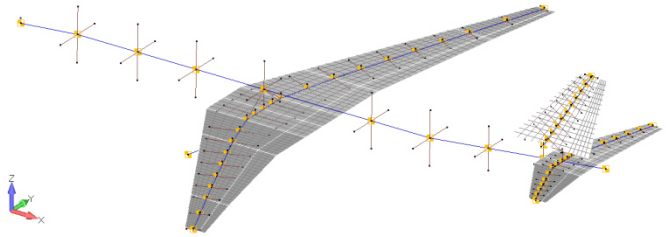

Fig. 1. Aerostructural mesh of the aircraft model.

A list of the main symmetric flexible modes of the aircraft, computed by a free-free normal modes analysis, is presented in Table 2. Rigid body modes are included too; these are zero-frequency modes as computed by Nastran. This approximation is deemed adequate for the present model since the separation between the phugoid and short-period modes and the first elastic modes is sufficient to prevent any interaction.

Table 2. Main symmetric flexible modes of the free-free aircraft

Mode #	Frequency [Hz]	Description
7	1.81	1st wing bending
9	2.61	1st wing bending + engine pitching
10	2.65	1st wing bending + engine yawing
13	3.64	2nd wing bending + horizontal tail bending
16	4.21	3rd wing bending + horizontal tail bending
19	5.05	3rd wing bending + fuselage bending

22	6.14	1st wing in-plane bending
23	7.96	1st wing torsion + 3rd wing bending
29	11.14	2nd wing torsion + 4th wing bending

3. Aeroelastic equations of motion

The linear aeroelastic equations of motion in generalized coordinates, excited by atmospheric gust, are formulated in the Laplace domain using the standard formulation [5] as

$$\left(s^2\boldsymbol{M_{hh}} + s\boldsymbol{C_{hh}} + \boldsymbol{K_{hh}} - q_\infty \boldsymbol{Q_{hh}}(p,M)\right)\boldsymbol{q_h}(s) = q_\infty \boldsymbol{Q_{hg}}(p,M)w_g(s)/V + q_\infty \boldsymbol{Q_{hc}}(p,M)\boldsymbol{\delta}(s) \tag{1}$$

where the generalized coordinates $\boldsymbol{q_h}$ could be either a low-frequency subset of the normal modes of the structure or a finite number of assumed deformation shapes.
The Generalized Aerodynamics Forces (GAF) matrices $\boldsymbol{Q_{hh}}$, $\boldsymbol{Q_{hg}}$ and $\boldsymbol{Q_{hc}}$ related respectively to structural motion, gust and control surfaces deflection, can be obtained by an unsteady aerodynamic code, such as the DLM, and are tabulated at specific Mach numbers and reduced frequencies k, i.e. along the imaginary axis of the complex reduced frequency $p = g + ik = sl_a/V$. The gust velocity profile w_g represents the external excitation.
The effects of the servo-hydraulic actuators driving the control surfaces are included assuming a 3rd order transfer function between the commanded input of the pilot u_c and the actual control surface deflection δ [14] such that

$$H_c(s) = \frac{\delta}{u_c} = \frac{k_c G_h(s)}{1 + k_c G_h(s)} \tag{2}$$

$$G_h(s) = \frac{k_h \omega_h^2}{s\left(s^2 + 2\zeta_h \omega_h s + k_h \omega_h^2\right)} \tag{3}$$

where $G_h(s)$ is the open-loop transfer function of the hydraulic actuator and k_c the gain of a position proportional controller. Under this modelling assumption, the actuators act as a shaping filter of the pilot input command, that is they introduce delays and overshoots in the actual control surfaces deflections following the pilot input at the stick.
The aeroelastic equations of motion can be directly solved in the frequency domain and the time histories of the IQs obtained through application of the Inverse Fourier Transform. To apply the Parametric Model Order Reduction method presented in this paper however, Eq. (1) must be translated into the time domain and cast in state-space form, leading to a Linear Time Invariant (LTI) system

$$\dot{\boldsymbol{x}}_{\boldsymbol{ae}} = \boldsymbol{A_{ae}}\boldsymbol{x_{ae}} + \boldsymbol{B_{ae}}\boldsymbol{u} \tag{4}$$

$$\boldsymbol{y} = \boldsymbol{C_{ae}}\boldsymbol{x_{ae}} + \boldsymbol{D_{ae}}\boldsymbol{u} \tag{5}$$

Since the GAF matrices are only available at a discrete set of reduced frequencies, in order to obtain a time domain representation of the aeroelastic system, the tabulated GAF matrices are used to compute a Rational Function Approximation (RFA) of the aerodynamics in the entire Laplace domain, which is given by

$$\widetilde{\boldsymbol{Q_{hh}}}(s,M) = \boldsymbol{D_0} + \frac{l_a}{V}\boldsymbol{D_1}s + \left(\frac{l_a}{V}\right)^2 \boldsymbol{D_2}s^2 + \boldsymbol{C_a}\left(s\boldsymbol{I} - \frac{V}{l_a}\boldsymbol{A_a}\right)\boldsymbol{B_a}s \tag{6}$$

$$\widetilde{\boldsymbol{Q_{hg}}}(s,M) = \boldsymbol{D_{0g}} + \frac{l_a}{V}\boldsymbol{D_{1g}}s + \left(\frac{l_a}{V}\right)^2 \boldsymbol{D_{2g}}s^2 + \boldsymbol{C_g}\left(s\boldsymbol{I} - \frac{V}{l_a}\boldsymbol{A_g}\right)\boldsymbol{B_g}s \tag{7}$$

Eqs. (6)-(7) result in the augmented aerodynamic state vectors $\boldsymbol{x_a}$ and $\boldsymbol{x_g}$ and the matrices in Eq. (4) are

$$\boldsymbol{A_{ae}} = \begin{bmatrix} \boldsymbol{0} & \boldsymbol{I} & \boldsymbol{0} & \boldsymbol{0} \\ -\boldsymbol{M_{ae}^{-1}}(\boldsymbol{K_{hh}} - q_\infty \boldsymbol{D_0}) & -\boldsymbol{M_{ae}^{-1}}(\boldsymbol{C_{hh}} - q_\infty \frac{l_a}{V}\boldsymbol{D_1}) & q_\infty \boldsymbol{M_{ae}^{-1}}\boldsymbol{C_a} & \boldsymbol{M_{ae}^{-1}}\boldsymbol{C_g} \\ \boldsymbol{0} & \boldsymbol{B_a} & \frac{V}{l_a}\boldsymbol{A_a} & \boldsymbol{0} \\ \boldsymbol{0} & \boldsymbol{0} & \boldsymbol{0} & \frac{V}{l_a}\boldsymbol{A_g} \end{bmatrix} \tag{8}$$

$$\boldsymbol{B_{ae}} = q_\infty \begin{bmatrix} \mathbf{0} & \mathbf{0} \\ \boldsymbol{M_{ae}^{-1} D_{0g}} & \boldsymbol{M_{ae}^{-1} \frac{l_a}{V} D_{1g}} \\ \mathbf{0} & \mathbf{0} \\ \mathbf{0} & \boldsymbol{B_g} \end{bmatrix} \tag{9}$$

with $\boldsymbol{M_{ae}} = \boldsymbol{M_{hh}} - q_\infty (l_a/V)^2 \boldsymbol{D_2}$ and $\boldsymbol{D_{2g}}$ assumed to be zero [15] to avoid the second time derivative of the gust velocity, which may be unsuitable when the excitation is continuous turbulence as it can introduced a white-noise derivative into the model.
The unsteady GAF of the control surfaces are instead cast into time-domain through a quasi-steady approximation, which reads

$$\widetilde{\boldsymbol{Q_{hc}}}(s, M) = \boldsymbol{D_{0c}} + \tfrac{l_a}{V}\boldsymbol{D_{1c}} s + \left(\tfrac{l_a}{V}\right)^2 \boldsymbol{D_{2c}} s^2 = \boldsymbol{Q_{hc}}(0, M) + \tfrac{l_a}{V}\boldsymbol{Q'_{hc}}(0, M) s + \tfrac{1}{2}\left(\tfrac{l_a}{V}\right)^2 \boldsymbol{Q''_{hc}}(0, M) s^2 \tag{10}$$

This choice is justified by the fact that the control surfaces input signals have a low frequency content, being limited by the pilot's bandwidth.
The control surface deflections are linked to the pilot input command u_c via the transfer function Eq. (3). Expressing the state-space realization of Eq. (2) in controllable canonical form adds three states to the aeroelastic system and the input vector $\boldsymbol{u}$ thus contains the gust velocity w_g, its first time derivative $\dot{w}_g$ and the pilot commanded input u_c. The output vector $\boldsymbol{y}$ contains the IQs, which are recovered through the mode displacement method.

3.1. Extended Rational Function Approximation Approach

Many approaches have been developed to perform the approximation of the tabulated GAF by rational polynomials in the Laplace domain [16],[17],[18],[19]. In this work, Roger's method [16] is used, which assumes the following representation of Eq. (6)

$$\widetilde{\boldsymbol{Q_{hh}}}(s, M) = \boldsymbol{D_0} + \tfrac{l_a}{V}\boldsymbol{D_1} s + \left(\tfrac{l_a}{V}\right)^2 \boldsymbol{D_2} s^2 + \tfrac{V}{l_a} \Sigma_{l=1}^{n_a} \frac{s}{s + V/l_a \beta_l} \boldsymbol{A_l} \tag{11}$$

In the original formulation, the number and values of aerodynamic poles β_l are fixed a-priori by the user in the range of reduced frequencies of interest, imposing that $\beta_l > 0$ to ensure asymptotic stability, and the unknowns are the coefficients of the matrices appearing at the numerator. These are determined by a linear least-square curve fit carried out term-by-term on each coefficient of the tabulated $\boldsymbol{Q_{hh}}$.
The GAF of the gust $\boldsymbol{Q_{hg}}$ is approximated independently with the same expression. This approach allows for a greater flexibility in the selection of gust aerodynamic poles and increases the fitting accuracy, an important consideration because the gust GAF is known to show a spiral behavior at high reduced frequencies in the Real-Imaginary plane, difficult to approximate with rational polynomials, due to the penetration term [15].
Although the choice of Roger's RFA and the independent fitting of the gust GAF leads to a state-space model whose size is greater compared to the Minimum-State method by Karpel [18], the model is afterwards reduced to a considerably smaller size through Model Order Reduction. Moreover, Roger's RFA is robust and offers less computational burden than the Minimum-State method [20], even though this cost, if a Model Order Reduction is not subsequently carried out, is ultimately overcome by the smaller resulting model employed in the simulations.
The original formulation by Roger hereby used is extended considering the aerodynamic poles as free design variables of an optimization process, whose objective function is the minimization of the squared error between the approximated and tabulated GAF. This approach gives an additional degree of freedom in obtaining good curve-fits, particularly for the gust GAF, for a small increase in computational cost. It also allows adapting the RFA to each Mach number of interest, since commonly, in the standard approach, the poles are held arbitrarily constant over a range of Mach numbers, whereas the GAF can change significantly with Mach number.
Several studies have been presented on nonlinear optimization of the aerodynamic poles [20],[21],[22],[23]. In this work, an optimization is performed to select the aerodynamic poles minimizing the functional $\mathcal{F}$ such that

$$\mathcal{F} = \sum_{j=1}^{n_h} \left(\sum_{i=1}^{n_h} \sum_{m=1}^{n_k} w_{ij} \varepsilon_{ijm} \right)^{1/2} \qquad \text{with residual} \tag{12}$$

$$\varepsilon_{ij} = \frac{|\widetilde{Q_{ij}} - Q_{ij}|^2}{max_m\{1, |Q_{ij}|^2\}} \tag{13}$$

where w_{ij} are weighting factors that can be chosen if some specific elements of the $\boldsymbol{Q_{hh}}$ are deemed more important to approximate accurately. The whole RFA procedure consists therefore of a two-level optimization: an inner linear least-square curve fitting for the coefficients matrices at the numerator of Eq. (11) and an outer nonlinear optimization for the aerodynamic poles β_l.
Because the aerodynamic poles appear in the denominator of Eq. (11), when these are chosen as variables in a gradient-based optimization method, there could be difficulties in computing the gradient and issues with the stability and convergence of the optimizer [21]. For this reason, three non-gradient optimization algorithms are employed and compared: a Nelder-Mead simplex scheme [24], a genetic algorithm [25] and simulated annealing [26].
As indicator of the goodness of the fit, the total root mean square error is calculated

$$RMSE = \frac{1}{\sqrt{n_k}} \sum_{j=1}^{n_h} \left(\sum_{i=1}^{n_h} \sum_{m=1}^{n_k} w_{ij} \varepsilon_{ijm} \right)^{1/2} \tag{14}$$

The standard and extended RFAs are performed on the aeroservoelastic model described in Section 2 from $\boldsymbol{Q_{hh}}$ and $\boldsymbol{Q_{hg}}$ generated by DLM at a Mach number of 0.60 for a range of reduced frequencies between 0 and 1.5, based on the frequency range that gust inputs can excite, and including the six aircraft rigid body modes.
Table 3 reports the total root mean square error of $\boldsymbol{Q_{hh}}$ obtained with the standard (unoptimized) RFA and the RFA with the aforementioned optimization algorithms assuming 5 aerodynamic poles. For the same number of aerodynamic states, there is a clear improvement of the approximation optimizing the poles location.

Table 3: Total approximation error and optimum aerodynamic poles of Q_{hh} for different RFA methods

RFA Method	RMSE	Aerodynamic poles	CPU time [s]
Standard	1.290E-03	0.057, 0.227, 0.510, 0.907, 1.417	1.3
Nelder-Mead	6.422E-04	0.520, 0.689, 0.741, 0.999, 1.001	3.2
Genetic Algorithm	5.309E-04	0.633, 0.784, 0.869, 1.041, 1.106	88.5
Simulated Annealing	5.135E-04	0.698, 0.899, 0.932, 0.973, 1.189	66.1

The curve fit of four elements of $\boldsymbol{Q_{hg}}$, computed with the same four approaches and assuming 6 aerodynamic poles, is presented in Fig. 2; the total root mean square error and the resulting aerodynamic poles are given in Table 4, alongside with the computational time required. Due to the spiral nature of the gust GAF, the RFA is very sensitive to the poles selection, therefore an optimization is particularly advantageous and improves significantly the curve fitting. In terms of computational effort, the Nelder-Mead algorithm is the most efficient one; however for all the methods, the additional computational time required compared to the standard RFA is still acceptable since this procedure must be carried out just once per Mach number in a pre-processing phase. Similar results are found for different Mach number cases.

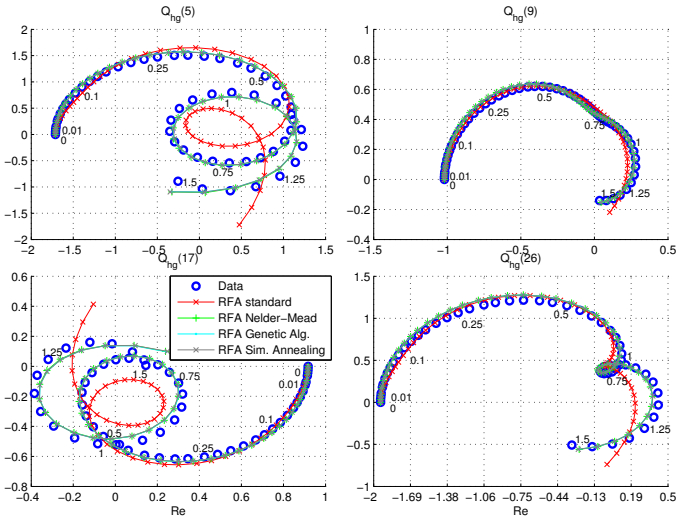

Fig. 2. Curve fits for different methods of four Q_{hg} terms at Mach 0.60

Table 4. Total approximation error and optimum aerodynamic poles of Q_{hg} for different RFA methods

RFA Method	RMSE	Aerodynamic poles	CPU time [s]
Standard	6.716E-01	0.032, 0.128, 0.289, 0.513, 0.802, 1.154	0.8
Nelder-Mead	2.211E-01	0.662, 0.663, 0.668, 0.670, 0.689, 0.693	2.5
Genetic Algorithm	2.228E-01	0.652, 0.658, 0.668, 0.682, 0.683, 0.708	22.2
Simulated Annealing	2.257E-01	0.570, 0.616, 0.626, 0.752, 0.769, 0.770	15.2

4. Generalized coordinates for aeroelastic analysis with structural modifications

The classical modal approach for model reduction, commonly employed in aeroelasticity, assumes that the displacements, and hence all the interesting quantities, are accurately represented by a linear combination of a low-frequency subset of the normal modes of the structure. When structural modifications occur, the normal modes and natural frequencies consequently change and repeated analyses are needed to find the new modal basis; as the model size increases, this process becomes time-consuming. A more efficient way is to use a fixed basis $\boldsymbol{T}$ for all the structural configurations and to form the aeroelastic system of Eq. (1) using generalized coordinates related to this basis.

Structural modifications can be represented by additive mass and stiffness matrices, respectively $\boldsymbol{\Delta M}$ and $\boldsymbol{\Delta K}$, to be added to the baseline mass and stiffness. The system of Eq. (1) is generated by projecting the mass and stiffness matrices of the modified structure onto the subspace spanned by $\boldsymbol{T}$, i.e.

$$\boldsymbol{M_{hh} = T^T(M + \Delta M)T} \tag{15}$$

$$\boldsymbol{K_{hh} = T^T(K + \Delta K)T} \tag{16}$$

Likewise, the matrices $\boldsymbol{Q_{AA}}$, representing the aerodynamic forces on each structural DOFs due to the displacement of the structural DOFs, and $\boldsymbol{Q_{Ag}}$, the aerodynamic forces on each structural DOFs due to the gust, are reduced by the basis $\boldsymbol{T}$.

$$\boldsymbol{Q_{hh} = T^T Q_{AA} T} \tag{17}$$

$$\boldsymbol{Q_{hg} = T^T Q_{Ag}} \tag{18}$$

Various bases have been proposed, the simplest ones being to use the normal modes of the nominal structure or a linear combination of these. One solution successfully employed in aeroelasticity is the fictitious mass method [27], which has been used as a global basis for aeroelastic analyses with structural modifications in [28].

In this work, the basis $\boldsymbol{T}$ is built following a multi-model approach [29], where the baseline modes and the modes of the modified structure at a number of representative design points in the parameter space are retained. These additional design points are selected by perturbing independently each of the n_d design parameter to their upper limit, with the others being kept constant at their nominal value. Multiple eigenvalue analyses are thereafter performed to calculate the low-frequency subsets of the normal modes of each of these n_d structural configurations, leading to the matrices of eigenvectors $\boldsymbol{\Phi_{p_i}}$, $i = 1 \dots n_d$.
In this way, the basis contains information on each parameter variation and is able to capture efficiently the dynamics of all the families of models generated inside the design space.
The total basis is thus obtained by appending n_d matrices of low-frequency normal modes of the perturbed structural configurations to the baseline one, $\boldsymbol{\Phi_0}$, such that

$$\boldsymbol{\Phi_{flex}} = \left[\boldsymbol{\Phi_0} \;\; \boldsymbol{\Phi_{p_1}} \dots \boldsymbol{\Phi_{p_{n_d}}}\right] \tag{19}$$

The computational saving is significant because $n_d + 1$ eigenvalue problems must be solved instead of a new one for each combination of parameters that is of interest for the aeroelastic response. This approach is hence particularly suitable when the number of analyses is much greater than the number of parameters, as often the case for structural optimization or uncertainties quantification.
Since the matrix formed by collecting all the design points' modes contains redundant information, due to many modes at the $n_d + 1$ structural configurations being almost linearly dependent, a SVD Eq. (20) is performed to remove the rank-deficient components and to retain only the directions with the highest energy. Rigid body modes $\boldsymbol{\Phi_{RB}}$ are then appended to the $\boldsymbol{U}_{1:n_h}$ retained flexible assumed mode shapes Eq. (21) and the basis $\boldsymbol{T}$ re-orthogonalized with respect to the mass and stiffness matrices of the baseline structure.

$$\boldsymbol{\Phi_{flex}} = \boldsymbol{U\Sigma Z^T} \tag{20}$$

$$\boldsymbol{T} = \left[\boldsymbol{\Phi_{RB}} \;\; \boldsymbol{U}_{1:n_h}\right] \tag{21}$$

5. Parametric Model Order Reduction

Model Order Reduction techniques have been applied in many engineering fields to replace expensive high fidelity models with low dimensional Reduced Order Models (ROM) that limit the complexity and computational cost of the simulations, but approximate well the underlying high dimensional systems.
For many engineering applications, the governing equations are parameterized and the solution needs to be computed over a potentially large range of parameter values. In the application considered here, the aeroelastic response of the aircraft must be solved to compute a large number of IQs under different flight conditions, mass configurations and external excitations to show compliance with the certification requirements or structural variations for uncertainties quantification. The parameters of the aeroelastic equations of motion are thus, for instance, the flight point, altitude and Mach number, and structural properties, such as engine mass or pylon stiffness. A considerable saving in computational effort can be made if, for the thousands of simulations required during an aircraft loads loop or for quantification of the effects of parameter uncertainties on the aeroelastic behaviour, a ROM is used in place of the high dimensional model. The ROM could thus be seen as a physics-based surrogate alternative to the data-fitting approaches, such as Kriging, Radial Basis Functions, Neural Networks or system identification proposed for the same purpose in [6],[7],[8]. Whereas a data-fit surrogate model, created in a black-box mode, maps an input/output relationship, a ROM embodies the underlying physics of the problem and, unlike the aforementioned methods, its validity is not limited to the conditions under which it was generated, but can be applied to simulate various initial conditions.
As the generation of a new ROM at each point of interest in the parameter space is usually impractical, and could even be more computationally expensive than building and evaluating the Full Order Model (FOM) anew, Parametric Model Order Reduction (PMOR) has been introduced to efficiently generate ROMs that preserve the parametric dependency and are accurate over a broad range of parameters, without the need of performing a new reduction at each design point.
A survey of the state-of-the-art in PMOR is given in [30], where various methodologies are presented and compared. To present the methodology applied in this work, the LTI state-space model of the aeroservoelastic system Eq. (4)-(5) is considered in the form

$$\dot{\boldsymbol{x}} = \boldsymbol{A}(\boldsymbol{p})\boldsymbol{x} + \boldsymbol{B}(\boldsymbol{p})\boldsymbol{u} \tag{22}$$

$$\boldsymbol{y} = \boldsymbol{C}(\boldsymbol{p})\boldsymbol{x} + \boldsymbol{D}(\boldsymbol{p})\boldsymbol{u} \tag{23}$$

where $\boldsymbol{p} \in \mathbb{R}^d$ is a set of parameters on which the state-space matrices arbitrarily depend and N is the order of the model. MOR seeks a low-dimensional approximation of this dynamic system, of order $n_r \ll N$, through a projection-based reduction

$$\dot{\boldsymbol{x}}_r = \boldsymbol{A}_r\boldsymbol{x}_r + \boldsymbol{B}_r\boldsymbol{u} \tag{24}$$

$$\boldsymbol{y} = \boldsymbol{C}_r\boldsymbol{x}_r + \boldsymbol{D}\boldsymbol{u} \tag{25}$$

where

$$\boldsymbol{A}_r = (\boldsymbol{W}^T\boldsymbol{V})^{-1}\boldsymbol{W}^T\boldsymbol{A}\boldsymbol{V} \tag{26}$$

$$\boldsymbol{B}_r = (\boldsymbol{W}^T\boldsymbol{V})^{-1}\boldsymbol{W}^T\boldsymbol{B} \tag{27}$$

$$\boldsymbol{C}_r = \boldsymbol{C}\boldsymbol{V} \tag{28}$$

The right and left projection matrices $\boldsymbol{W} \in \mathbb{R}^{N\,x\,n_r}$ and $\boldsymbol{V} \in \mathbb{R}^{N\,x\,n_r}$ are referred as the Reduced Order Bases (ROB) and the methods used to calculate these fall into three categories [31]:

- Krylov-Subspace methods
- Balanced Truncation
- Proper Orthogonal Decomposition

In this paper, the Balanced Truncation is chosen to compute the ROB as it is one of the most common techniques employed in the control systems field [32]. It has desirable properties such as stability preservation of the reduced models, an H_∞ error bound and the dimension of the ROM can be easily chosen by observing the Hankel singular values of the state-space system in balanced form. The right and left bases computed by Balanced Truncation are the inverse of each other, i.e. $\boldsymbol{W}^T = \boldsymbol{T}_{\boldsymbol{B}}$, $\boldsymbol{V} = \boldsymbol{T}_{\boldsymbol{B}}^{-1}$ and $\boldsymbol{W}^T\boldsymbol{V} = \boldsymbol{I}$.
The idea behind a PMOR is to generate the ROB at few selected sampling points $\hat{\boldsymbol{p}}_{\boldsymbol{i}}$ (referred to as local ROBs/ROMs) in the parameter domain and then construct a Parametric Reduced Order Models (PROM) at all the other points of interest. Several approaches are possible for this second part:

1. Assemble a global basis by collecting the local ROB computed at $\hat{\boldsymbol{p}}_{\boldsymbol{i}}$ and use this basis to reduce the FOM over the parameter space
2. Interpolate the local ROB to the new unsampled point $\overline{\boldsymbol{p}}$ and perform the reduction
3. Interpolate the locally reduced transfer functions to the new unsampled point $\overline{\boldsymbol{p}}$
4. Interpolate the locally reduce state-space matrices to the new unsampled point $\overline{\boldsymbol{p}}$

The first two approaches are more appropriate if the system has an affine parameter dependency, i.e. the matrices can be explicitly expressed as

$$\boldsymbol{A}(\boldsymbol{p}) = \boldsymbol{A}_{\boldsymbol{0}} + \sum_{i=1}^{m} f_i(\boldsymbol{p})\boldsymbol{A}_{\boldsymbol{i}} \tag{29}$$

so that the reduced matrices are quickly computed at each $\overline{\boldsymbol{p}}$ and the construction and subsequent reduction through projection of a new FOM is avoided. The interpolation of the locally reduced transfer functions, and of the locally reduced state-space matrices, do not suffer from this limitation and thus are more convenient for a generic non-affine parameter dependency, which is indeed the case of the aeroservoelastic system of Eq. (1).
In this work the approach of PMOR by state-space matrices interpolation is chosen. This method has been successfully applied in the past in aeroelasticity, for fast flutter clearance of a wing-store configuration [33], in control system design of a flexible aircraft [34], in unsteady CFD [35] and in other engineering domains [36], but not for gust and manoeuvre loads prediction. Hereafter, the PMOR framework proposed in [37] is followed. It consists of the following steps:

1. Generation of the n_p local ROMs at the sampling points $\widehat{\boldsymbol{p}}_{\boldsymbol{i}}$, $i = 1 \dots n_p$
2. Congruence transformation of the locally reduced state-space matrices
3. Elementwise interpolation of the locally reduced state-space matrices to the validation points $\overline{\boldsymbol{p}}$
4. Time simulation of the resulting interpolated ROM

In the first step, the parameter space is sampled, the FOMs constructed at each of these points and then individually reduced through Balanced Truncation. All the local ROMs have the same order n_r. For the aeroservoelastic system under consideration this task is quite challenging because the state matrix is poorly conditioned, lightly damped and neutrally stable poles are present (rigid body modes). Moreover, to achieve a significant computational time saving, the sampling grid must be coarse, whereas the altitude and airspeed affect considerably the dynamics of the aircraft. As the Balanced Truncation is not a physics-based reduction, the states of the ROMs at different parameter values lie in unrelated subspaces and, before the interpolation, must be transformed, through a similarity transformation $\boldsymbol{x}_{\boldsymbol{r},\boldsymbol{i}} = \boldsymbol{P}_{\boldsymbol{i}}\widehat{\boldsymbol{x}_{\boldsymbol{r},\boldsymbol{\iota}}}$, to a congruent common subspace, spanned by the column of the matrix $\boldsymbol{R} \in \mathbb{R}^{N\,x\,n_r}$. The choice of this reference subspace is critical for the accuracy of the entire procedure; it is problem-dependent and various options have been proposed [30],[34]. A solution that, for the application considered, is robust and delivers accurate results is adopting the first n_r singular vectors of the matrix $\boldsymbol{V}_{\boldsymbol{all}}$ as the reference subspace $\boldsymbol{R}$ **,** a process which collects all the local ROB so that $\boldsymbol{V}_i = \boldsymbol{T}_{\boldsymbol{B},\boldsymbol{i}}^{-1}$, and hence

$$\boldsymbol{V}_{\boldsymbol{all}} = \left[\boldsymbol{V}_{\boldsymbol{1}}\ \boldsymbol{V}_{\boldsymbol{2}} \dots \boldsymbol{V}_{\boldsymbol{n_p}}\right] \tag{30}$$

$$\boldsymbol{V}_{\boldsymbol{all}} = \boldsymbol{U}\boldsymbol{\Sigma}\boldsymbol{Z}^T \tag{31}$$

$$\boldsymbol{R} = \boldsymbol{U}_{1:n_r} \tag{32}$$

where first the matrices $\boldsymbol{T}_{\boldsymbol{B},\boldsymbol{i}}^{-1}$ are orthonormalized to limit the loss of accuracy due to this further transformation. The transformation matrix $\boldsymbol{P}_i$, for each local ROM, is computed by solving the minimization problem [30]

$$\min_{\boldsymbol{P}_i} \|\boldsymbol{V}_i\boldsymbol{P}_i - \boldsymbol{R}\|_F^2 \qquad s.t.\ \ \boldsymbol{P}_i{}^T\,\boldsymbol{P}_i = \boldsymbol{I} \tag{33}$$

This minimization problem can be interpreted as a weak fulfillment of the Modal Assurance Criterion (MAC) between the columns of the subspace spanned by $\boldsymbol{R}$ and those of the subspace spanned by the congruent transformed reduced basis $\widehat{\boldsymbol{V}_\iota} = \boldsymbol{V}_i\boldsymbol{P}_i$ [38]. The solution to Eq. (30) is obtained through a SVD such that

$$\boldsymbol{U}_{\boldsymbol{V}_i}\boldsymbol{\Sigma}_{\boldsymbol{V}_i}\boldsymbol{Z}_{\boldsymbol{V}_i}^T = svd(\boldsymbol{V}_i\boldsymbol{R}) \tag{34}$$

$$\boldsymbol{P}_i = \boldsymbol{U}_{\boldsymbol{V}_i}\boldsymbol{Z}_{\boldsymbol{V}_i}^T \tag{35}$$

The congruence transformed local ROM are given by the expressions

$$\widehat{\boldsymbol{A}_{\boldsymbol{r},\boldsymbol{\iota}}} = \boldsymbol{P}_i{}^T\boldsymbol{T}_{\boldsymbol{B}}\boldsymbol{A}(\widehat{\boldsymbol{p}}_{\boldsymbol{i}})\boldsymbol{T}_{\boldsymbol{B},\boldsymbol{i}}^{-1}\boldsymbol{P}_i \tag{36}$$

$$\widehat{\boldsymbol{B}_{\boldsymbol{r},\boldsymbol{\iota}}} = \boldsymbol{P}_i{}^T\boldsymbol{T}_{\boldsymbol{B}}\boldsymbol{B}(\widehat{\boldsymbol{p}}_{\boldsymbol{i}}) \tag{37}$$

$$\widehat{\boldsymbol{C}_{\boldsymbol{r},\boldsymbol{\iota}}} = \boldsymbol{C}(\widehat{\boldsymbol{p}}_{\boldsymbol{i}})\boldsymbol{T}_{\boldsymbol{B},\boldsymbol{i}}^{-1}\boldsymbol{P}_i \tag{38}$$

Once all the local reduced models are available in this form, the resulting PROM at $\overline{\boldsymbol{p}}$ is obtained by direct interpolation of the matrices in Eq. (36)-(38). The interpolation is performed element-by-element through a linear or cubic spline interpolant. This step is the other main source of inaccuracy of the procedure, besides the reduction itself.

6. Application to gust and manoeuvre loads prediction

Certification requirements specify the discrete gust load cases considering the aircraft in level flight subject to symmetrical vertical and lateral gusts with a "1-cosine" velocity profile having gust gradient *H* (half of the gust wavelength) and asking for several gust gradients between 30ft and 350ft to be investigated in order to determine the

critical conditions [1],[5]. The certification specifications also cover unchecked and checked abrupt pitching manoeuvres [1],[5] resulting from either a sudden or sinusoidal displacement of the elevator.
The PROM methodology presented was applied to first simulate all the gust and pitching manoeuvre load cases across the flight envelope (altitude vs. Mach) and then to efficiently calculate loads following structural modifications of the engine mass and pylon stiffness. To assemble the state-space model Eq. (4)-(5) for the flight envelope sweep, the first 30 normal modes were retained, based on a convergence study of the wing and horizontal tail loads, and the RFAs of $\boldsymbol{Q_{hh}}$ and $\boldsymbol{Q_{hg}}$ performed with respectively 5 and 6 aerodynamic poles optimized using a Genetic Algorithm. The total aeroelastic state-space model features 390 states and three inputs, namely gust velocity and its time derivative and pilot elevator command. For structural modifications applications, the generalized basis was assembled considering the 31 assumed shapes computed as described in Section 4, leading to a model with 403 states. The number of assumed shapes has been selected following a convergence study on the wing engine section and pylon loads (bending moment, shear and torque), being these the components most affected by the considered structural modifications.

6.1. Flight envelope sweep

For the first application altitude and Mach number were considered as parameters of the PROM to compute gust and pitching manoeuvre loads covering the whole flight envelope.
The 16 flight conditions (sampling points) were generated using a full-factorial design, taking as the range of the 2D parameter space the minimum and maximum Mach numbers and minimum and maximum altitudes and used to generate the ROMs for the interpolation are shown in Fig. 3, along with the 156 conditions used to sweep the whole flight envelope (validation points). Through Balanced Truncation, the number of states is reduced from 390 to 34.
The reduced state-space matrices are interpolated elementwise through a simple yet efficient bilinear interpolant and FOMs are constructed at each validation point to assess the accuracy of the procedure. Time simulations of the gust response, considering ten gust gradients chosen to cover evenly the entire range defined by the airworthiness regulations (9m – 107m) [1],[34], and pitching manoeuvres are then carried out using a state-transition matrix integration method.

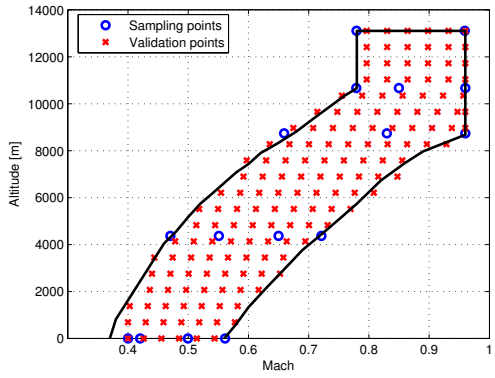

Fig. 3. Sampling points and validation points in the flight envelope

To assess the accuracy of the procedure, the errors, with respect to the FOM, of the maximum and minimum wing root bending moment and wing engine inboard section vs. Mach number and altitude are presented in Fig. 4. The predictions are very good, the error in the whole flight envelope being less than ±3%. The accuracy is slightly worse for the torque because the torsional modes have higher frequencies than the bending modes and are hence more sensitive to the states truncation. Similarly, shorter gusts, which excite a higher frequency range, result in greater approximation errors. Note, however, that the errors relating to higher frequencies are caused by the balanced truncation itself rather than by the interpolation of the locally reduced models.

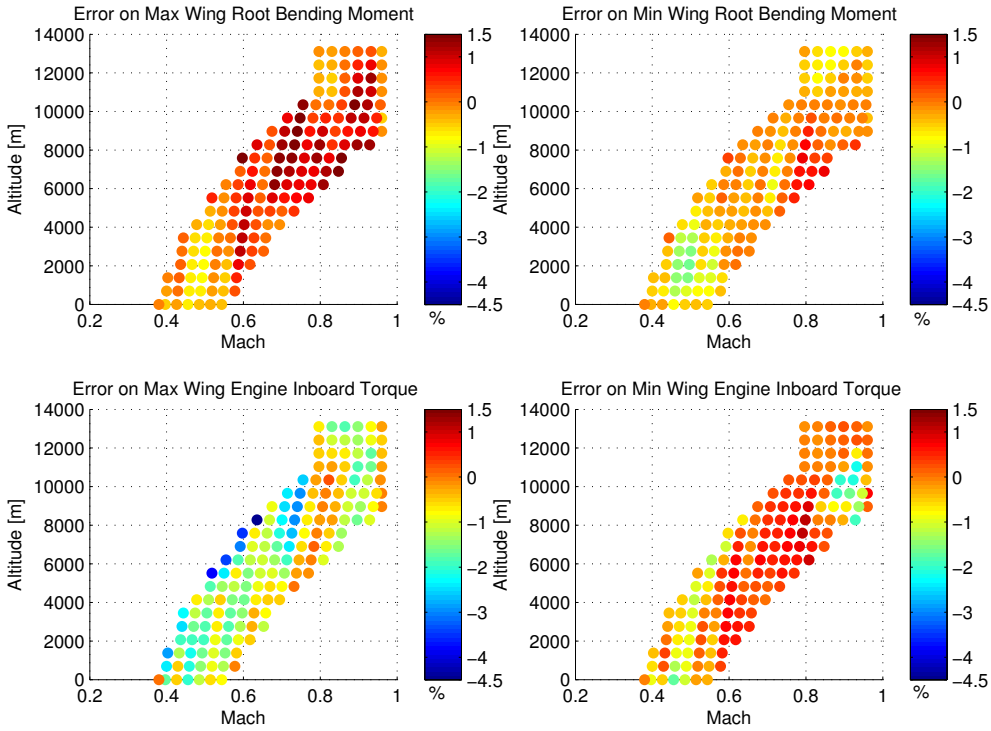

Fig. 4. Percentage error on the Max/Min prediction of the wing root bending moment and wing engine inboard torque

The approximation errors are in line with those presented in [7],[8], where Neural Networks and system identification were used as black-box surrogates to approximate the extreme responses. However, following those approaches, a different metamodel must be built for each IQ, a cost that could quickly become unacceptable for an industrial case where thousands of IQs are monitored. The present methodology is much more flexible since this need is achieved by simply adding a row in the $\boldsymbol{C}$ and $\boldsymbol{D}$ matrices of the output equations. In addition, the number of sampling points required to generate an accurate PROM is considerably lower than that needed by data-fit surrogates [6].

A convergence study has been performed on the number of sampling points and is presented in Fig. 5. This shows the maximum magnitude of the errors (either positive or negative) on the maximum wing root bending moment and wing engine inboard torque. It can be noted that the trend is decreasing and monotonic with the number of sampling points, as expected, and that the selected set of 16 points is a good tradeoff between achieving accuracy, as the errors are near convergence, and limiting the computational cost, which is proportional to the number of samples.

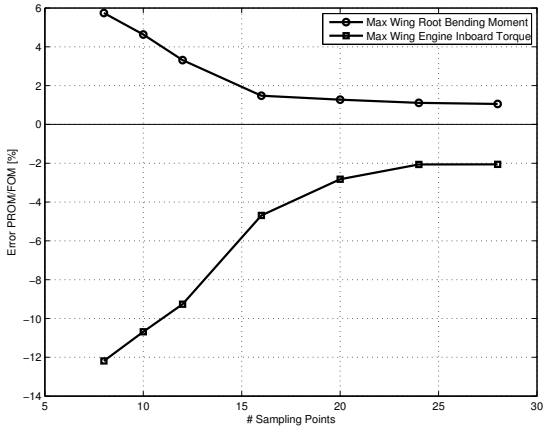

Fig. 5. Percentage error on maximum wing root bending moment and engine inboard torque vs. number of sampling points

A more challenging goal is the efficient approximation of correlated loads plots. Fig. 6 shows the correlated loads plots, bending moment vs. torque, of a gust family at the root and inboard engine wing sections obtained with the FOM and the PROM at two flight conditions. The prediction obtained with the PROM, as for 1D IQs, is in excellent agreement with the FOM computations.

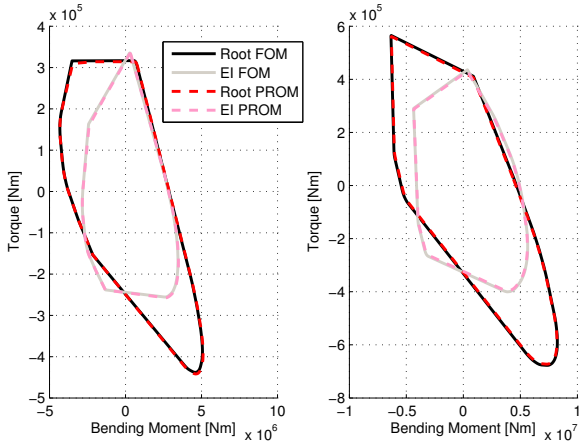

Fig. 6. Correlated loads plots at the wing root and inboard engine wing section at h=0m-M=0.48 (left) and h=6208m-M=0.74 (right), FOM vs. PROM

Similarly, simulations of unchecked and checked abrupt pitching manoeuvres are performed with the PROM and FOM. The time histories of the load factor during a nose-up and nose-down checked pitching manoeuvre are shown in Fig. 7, for a specific flight condition, alongside with the bending moment and torque at the horizontal tail root. A very good matching can be obtained for these load cases too, as confirmed by the correlated loads plots of the wing root and horizontal tail root presented in Fig. 8.

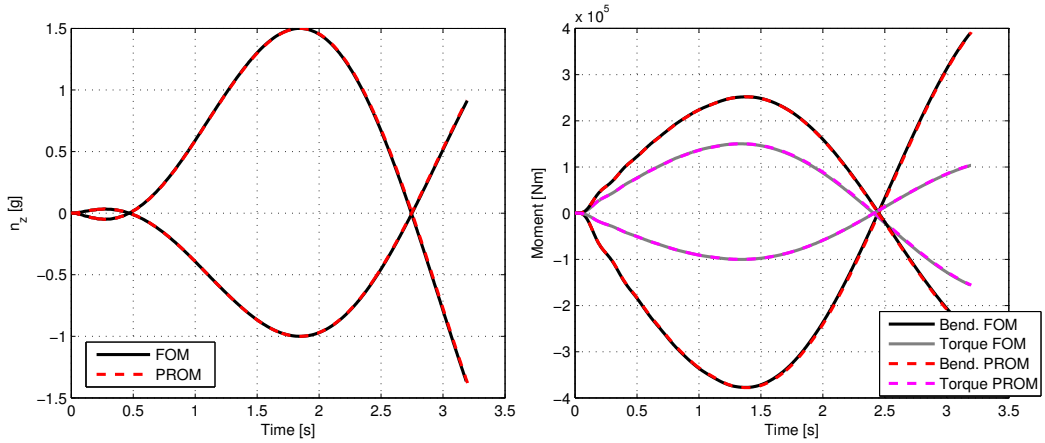

Fig. 7. Load factor and horizontal tail root loads for nose-up and nose-down checked pitching manoeuvre at h=0m-M=0.40, FOM vs. PROM

The unchecked pitching manoeuvre must be performed up to V_A. The Max/Min IQ approximation error of the PROM over this reduced flight envelope is represented in Fig. 9 for the wing root bending moment and the horizontal tail root bending moment and torque. Again, as for gust responses, the error is below ±3% throughout the flight envelope.

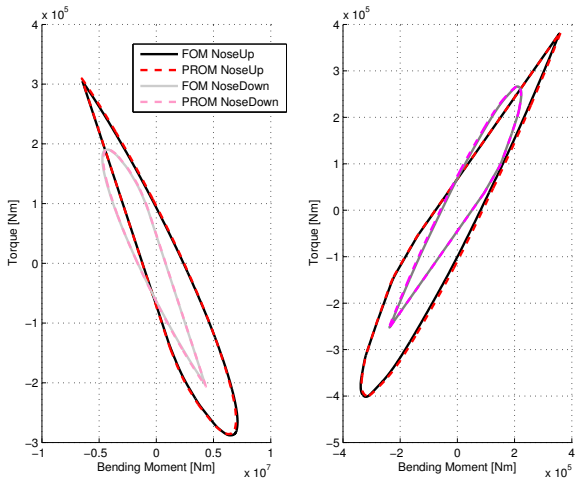

Fig. 8. Correlated loads plots at the wing root (left) and horizontal tail root (right) for nose-up and nose-down checked pitching manoeuvre at h=12417m-M=0.90, FOM vs. PROM

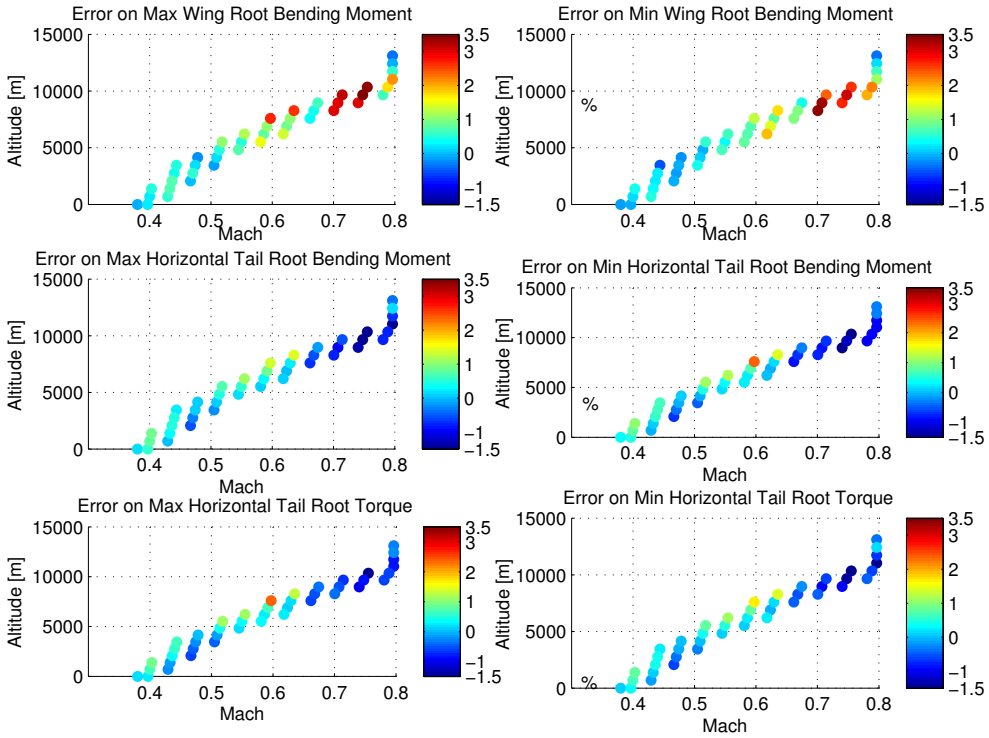

Fig. 9. Percentage error on the Max/Min prediction of the wing root bending moment and horizontal tail root bending moment and torque for unchecked pitching manoeuvre

For all the load conditions considered, the agreement between the FOM and PROM is excellent, demonstrating thus that the proposed method can deliver accurate predictions for a considerable saving in computational effort. The saving increases with the number of simulations to be performed: for the complete sweep of the flight envelope, considering ten gust gradients, the speed-up factor exceeds 9 (Table 5).

A breakdown of the computational time is presented in Table 6. Whereas for the FOM most of the computational time is spent performing the time simulation, for the PROM this makes up only 34% of the total time, the greatest part being spent in the calculation of the balanced truncation of the state-space models at the sampling points.

Table 5. Speed-up factor vs. number of gust simulations

Num. Simulations	Speed-up factor
500	2.5
1000	4.5
1500	6.67
2500	9.1

Table 6. Computational time breakdown of FOM and PROM

Phase	FOM	PROM
Model generation and reduction	6%	63%
Congruence transformation	--	1%
Interpolation	--	2%
Simulation	94%	34%

6.2. Rapid gust loads prediction under structural modifications

A second application deals with the prediction of correlated gust loads under structural modifications. The structural parameters considered are the engine mass and the pylon stiffness, specifically the first is assumed to vary around its nominal value by ±10% and the second by ±20%. The airspeed and altitude are varied too, leading to a 4D parameter space. The FOM is reduced through balanced truncation to 34 states at 128 sampling points, generated by full-factorial design, and a spline interpolant is employed to obtain the coefficients of the reduced state-space matrices at the validation points.The response surfaces of the maximum and minimum wing root and wing inboard engine section torque vs. engine mass and pylon stiffness variations, at one flight condition (Mach 0.60, altitude 7500m) and gust gradient (105ft), are shown in Fig. 10. Fig. 11 presents the correlated loads plots of the entire gust family at the wing inboard engine section obtained with the FOM and the PROM for two structural variations and flight conditions (LC#1 h=6553m-M=0.40, +5% engine mass, +10% pylon stiffness; LC#2 h=6553m-M=0.67, +10% engine mass, -10% pylon stiffness).
The effect of the structural modifications is an increase in torque with higher engine mass and lower pylon stiffness. This is expected as the torque is mainly generated by the inertia forces of the engine, which increase for a higher mass and for a lower stiffness due to the higher accelerations experienced.

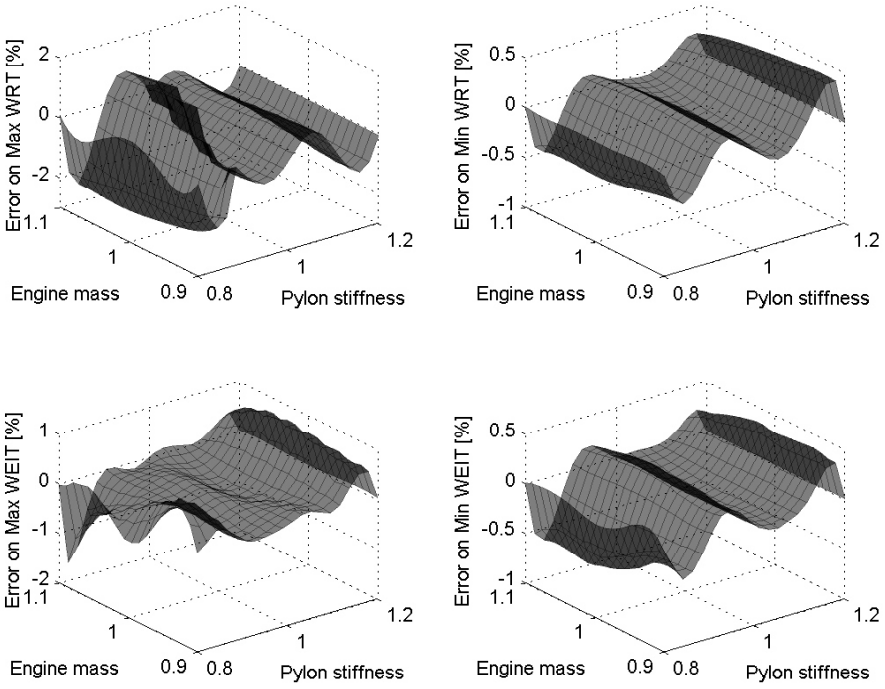

Fig. 10. Response surfaces of the error (PROM with respect to FOM) of the maximum and minimum wing root and wing inboard engine torque vs. engine mass and pylon stiffness.

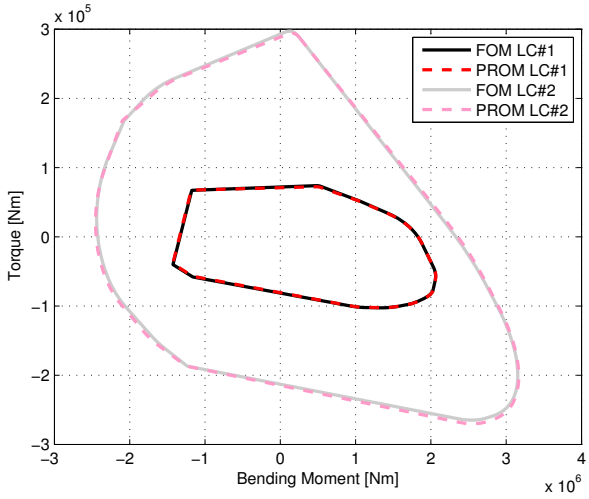

Fig. 11. Correlated loads plots at the wing inboard engine section for two load cases, FOM vs. PROM

As in the previous application, the results are in good agreement even with the larger parameter space formed by altitude, Mach number, engine mass and pylon stiffness. Similar results were found for different gust gradients. The PROM procedure is therefore capable of handling a multi-dimensional parameter dependency and of delivering accurate predictions with reduced computational effort.

7. Conclusions

A method based on a Parametric Reduced Order Model has been applied to rapidly predict gust and manoeuvre loads of a transport aircraft aeroservoelastic model. Both different flight conditions and structural parameter variations have been considered. The equations of motion are formulated in state-space, through an improved Rational Function Approximation of the frequency domain aerodynamic forces, using a unique generalized basis for different structural configurations. The approach enables efficient prediction of the peak loads whilst maintaining the correlated time histories for different loads. It is then possible to determine correlated loads plots with reduced computation without losing accuracy.

The effectiveness of the methodology is demonstrated by considering loads arising from families of gusts and pitching manoeuvres acting upon a numerical transport aircraft aeroservoelastic model with varying flight conditions and structural properties. It is shown that both Max/Min and correlated loads are accurately predicted achieving a significant saving in computational time.

Acknowledgements

This work is supported by the European Commission (EC FP7) under the Marie Curie European Industrial Doctorate Training Network ALPES (Aircraft Loads Prediction using Enhanced Simulation – Grant Agreement No. 607911) and the Royal Academy of Engineering.

References

[1] EASA, Certification Specification for Large Aeroplanes CS-25 Amendment 3, September 2007.

[2] Zeiler T. A., Matched Filter Concept and Maximum Gust Loads, J. Aircr. 34 (1) (1997) 101-108.

[3] Jones J. G., Statistical Discrete Gust Method for Predicting Aircraft Loads and Dynamic Response J. Aircr. 26 (4) (1989) 382-392.

[4] Karr C. L. Zeiler T. A., and Mehrotra R., Determining Worst Case Gust Loads on Aircraft Structures using an Evolutionary Algorithm, Appl. Intell. 20 (2004) 135-145.

[5] Wright J. R., and Cooper J. E., Introduction to Aircraft Aeroelasticity and Loads, Wiley, 2007.

[6] Khodaparast, H. H., Georgiou, G., Cooper, J. E., Riccobene, L., Ricci, S., Vio, G. A., and Denner, P., Efficient Worst Case 1-Cosine Gust Loads Prediction, ASD Journal 2 (3) (2012) 33-54.

[7] Cavagna, L., Ricci, S., and Riccobene, L., FAST-GLD: a Fast Tool for the Prediction of Worst Case Gust Loads based on Neural Networks, Proc. of 54th AIAA/ASME/ASCE/AHS/ASC Structures, Structural Dynamics and Materials Conference, Boston, 2013.

[8] Khodaparast, H. H., and Cooper, J. E., Worst Case Gust Loads Prediction Using Surrogate Models and System Identification Methods, Proc. of 54th AIAA/ASME/ASCE/AHS/ASC Structures, Structural Dynamics and Materials Conference, Boston, 2013.

[9] Corman, J. A., Rancourt, D., Lee, C. H., Mavris, D. N., and Wilson, T., Preliminary Wing Weight Estimation Under Probabilistic Loads for a Transport Aircraft, Proc. of 55th AIAA/ASME/ASCE/AHS/ASC Structures, Structural Dynamics and Materials Conference, National Harbor, 2014.

[10] Tartaruga, I., Sartor, P., Cooper, J. E., Coggon, S., and Lemmens, Y., Efficient Prediction and Uncertainty Propagation of Correlated Loads, Proc. of 56th AIAA/ASME/ASCE/AHS/ASC Structures, Structural Dynamics and Materials Conference, Orlando, 2015.

[11] Knoblach A., Robust Performance Analysis Applied to Gust Loads Computations, ASD Journal 3 (1) (2013) 39-50.

[12] Albano, E., and Rodden, W. P., A Doublet-Lattice Method for Calculating Lift Distributions on Oscillating Surfaces in Subsonic Flows, AIAA J. 7 (2) (1969) 279-285.

[13] Harder, R. L., and Desmarais, R.N., Interpolation using Surface Splines, AIAA J. 9 (2) (1972) 189-191.

[14] Merrit, H. E., Hydraulic Control Systems, Wiley, 1967.

[15] Karpel, M., Moulin, B., and Chen, P. C., Dynamic Response of Aeroservoelastic Systems to Gust Excitation, J. Aircr. 42 (5) (2005) 1264-1272.

[16] Roger, K. L., Airplane Math Modeling Methods for Active Control Design, AGARD CP-228, 1977.

[17] Vepa, R., Finite-State Modeling of Aeroelastic Systems, NASA CR-2779, 1977.

[18] Karpel, M., Design for Active and Passive Flutter Suppression and Gust Alleviation, NASA CR-3482, 1981.

[19] Ripepi, M., and Mantegazza, P, Improved Matrix Fraction Approximation of Aerodynamic Transfer Matrices, AIAA J. 51 (5) (2013) 1156-1173.

[20] Tiffany, S. H., and Adams, W. M., Jr., Nonlinear Programming Extensions to Rational Function Approximation for Unsteady Aerodynamic Forces, NASA TP-2776, 1988.

[21] Eversman, W., and Tewari, A., Consistent Rational-Function Approximation for Unsteady Aerodynamics, J. Aircr. 28 (9) (1991) 545-552.

[22] Karpel, M., and Strul, E, Minimum-State Unsteady Aerodynamic Approximations with Flexible Constraints, J. Aircr. 33 (6) (1996) 1190-1196.

[23] Berci, M., Optimal Approximation of Indicial Aerodynamics, Proc. of the1st International Conference on Engineering and Applied Sciences Optimization, National Technical University of Athens, Athens, 2014.

[24] Luersen, M. A., Le Riche, R., and Guyon, F., A constrained, globalized, and bounded Nelder–Mead method for engineering optimization, Struct. Multidiscip. O. 27 (1-2) (2004) 43-54.

[25] Goldberg, D. E., Genetic Algorithms in Search, Optimization & Machine Learning, Addison-Wesley, 1989.

[26] Kirkpatrick, S., Gelatt, C. D., and Vecchi, M. P., Optimization by Simulated Annealing, Science 220 (4598) (1983) 671-680.

[27] Karpel, M., and Presente, E, Structural Dynamic Loads in Response to Impulsive Excitation, J Aircr. 32 (4) (1995) 853-861.

[28] Karpel, M., and Wieseman, C. D., Time Simulation of Flutter with Large Stiffness Changes, J. Aircr. 31 (2) (1994) 404-410.

[29] Balmes, E., Parametric families of reduced finite element models. Theory and applications, Mech. Syst. Signal Pr. 10 (4) (1996) 381-394.

[30] Benner, P., Gugercin, S., and Willcox, K., A Survey of Model Reduction Methods for Parametric Systems, Max Planck Institute Magdeburg Preprints, 2013.

[31] Antoulas, A. C., An Overview of Approximation Methods for Large-Scale Dynamical Systems, Ann. Rev. Contr. 29 (2) (2005) 181-190.

[32] Moore, B., Principal component analysis in linear systems: Controllability, observability and model reduction, IEEE T. Automat. Contr. 26 (1981) 17-32.

[33] Amsallem, D., and Farhat, C., Interpolation Method for the Adaption of Reduced-Order Models to Parameter Changes and its Application to Aeroelasticty, AIAA J. 46 (7) (2008) 1803-1813.

[34] Poussot-Vassal, C., and Roos, C., Generation of a reduced-order LPV/LFT model from a set of large-scale MIMO LTI flexible aircraft models, Control Eng. Pract. 20 (9) (2012) 919-930.

[35] Zimmermann, R., A Locally Parametrized Reduced-Order Model for the Linear Frequency Domain Approach to Time-Accurate Computational Fluid Dynamics, SIAM J. Sci. Comput. 36 (3) (2014) 508-537.

[36] Degroote, J., Vierendeels, J., and Willcox, K., Interpolation among reduced-order matrices to obtain parameterized models for design, optimization and probabilistic analysis, Int. J. Num. Meth. Fl. 63 (2010) 207-230.

[37] Panzer, H., Mohring, J., Eid, R., and Lohmann, B., Parametric Model Order Reduction by Matrix Interpolation, at-Automatisierungstechnik, 58 (8) (2010) 475-484.

[38] Geuss, M., Panzer, H., and Lohmann, B., On parametric Model Order Reduction by Matrix Interpolation, Proc. of the 2013 European Control Conference, Zurich, 2013.

Vitae

Michele Castellani

Michele Castellani obtained a MSc in Aeronautical Engineering from Politecnico di Milano in 2011. Following graduation, he joined Pilatus Aircraft Ltd., Switzerland, as a Loads Engineer in the Future Projects Department, working on the development and certification of the business jet PC-24. In May 2014 he joined Siemens PLM, Belgium, as a Research Engineer working in the EU FP7 Marie Curie project ALPES, a European Industrial Doctorate jointly organized by Siemens PLM and the University of Bristol devoted to the improvement of aircraft loads prediction. He is currently enrolled as a PhD candidate at the University of Bristol.

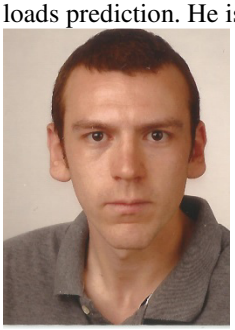

Yves Lemmens

Dr. Yves Lemmens has a degree Mechanical Engineering and in Aviation and Space Technologies from the University of Brussels. He has furthermore a Ph.D. from the Department of Aerospace Engineering of Cranfield University. He is currently a senior research project leader at Siemens PLM Software, where he leads a team of researchers that focus on multi-body and system simulation for aerospace applications. He is involved in several European and Belgian research projects, including the Scientist-in-Charge for Siemens in an EU Marie Curie project on Aircraft load and the Coordinator of an EU Clean Sky project on aircraft mechanisms.

Jonathan Cooper

Jonathan Cooper is the Airbus Royal Academy of Engineering Sir George White Professor of Aerospace Engineering at the University of Bristol. He has researched in the fields of aeroelasticity and structural dynamics for nearly 30 years, with over 250 technical publications and is also the co-author of the Wiley textbook on an Introduction to Aircraft Aeroelasticity and Loads. Prof Cooper is a Fellow of the RAeS and an Associate Fellow of the AIAA.